Tunable Optoelectronic Properties of Bilayer MoS$_2$ via Interlayer Twist and Uniaxial Strain

Weibin Zhang, Fanghua Cheng, Junwei Huang, and Quan Wang*

2D twisted layered materials provide a new platform to study strongly correlated quantum phenomena. In homo- or heterostructures, the interlayer coupling is sensitive to the twist angles (θ), which serves as a key order parameter to controllably adjust exotic properties therein. The widely studied atomically thin molybdenum disulfide (MoS$_2$) shows strong photoluminescence (PL) and is considered a promising optoelectronic material. Herein, by applying a uniaxial strain up to 5%, the evolution of the Raman and PL spectra of bilayer MoS$_2$ with four different twist angles is investigated. The redshift per unit strain of the PL energy in twisted bilayer MoS$_2$ (tBLM) reaches its extreme when θ is 30°. Further, two kinds of phototransistors based on tBLM structures with twist angles of 0° and 30° are constructed. The photoresponsivity (R) and the specific photodetectivity (D^*) of the 30°-twisted-tBLM-based phototransistor are successfully improved by $\approx$20 and $\approx$100 times than those values of the 0°-twisted one, respectively. These findings provide a beneficial understanding of the effects of twist angle and strain on the optical and electrical applications based on tBLM and are applicable to other 2D materials.

1. Introduction

Van der Waals (vdW) heterostructures have two important fabrication factors, including the types of constructive materials and their relative twist angle.[1–5] Atomically thin-twisted 2D materials can generate large-scale periodic moiré superlattices,[6] resulting in strongly correlated phenomena such as unconventional superconductivity and quantum phase transitions[7–13] due to the internal strain related to lattice distortion. Such lattice

W. Zhang, Q. Wang
Zhenjiang Key Laboratory of Advanced Sensing Materials and Devices
School of Mechanical Engineering
Jiangsu University
Zhenjiang 212013, P. R. China
E-mail: wangq@ujs.edu.cn

F. Cheng, J. Huang
College of Engineering and Applied Sciences
National Laboratory of Solid State Microstructures, and Jiangsu Key
Laboratory of Artificial Functional Materials
Nanjing University
Nanjing 210000, P. R. China

Q. Wang
State Key Laboratory of Transducer Technology
Chinese Academy of Sciences
Shanghai 200050, P. R. China

The ORCID identification number(s) for the author(s) of this article can be found under https://doi.org/10.1002/pssr.202200235.

distortion can also be significantly strengthened by applying an external mechanical strain.[14,15]

In recent years, interlayer twist has proven to be a convenient and effective method to change the interlayer coupling of the homo- and heterostructures of 2D materials. Compared with graphene, many monolayer transition metal dichalcogenides (TMDs) are semiconductors with bandgaps in the range of 1–2 eV, which makes these materials promising for optoelectronic applications.[16–19] Furthermore, the monolayer TMDs exhibit strong spin–orbit coupling due to the presence of heavy metal atoms and the characteristics of their crystal structure. As an important member of the TMD family, MoS$_2$ is an ideal semiconductor material. As with twisted grapheme,[20–22] it is also interesting to study the photoelectric properties of twisted MoS$_2$. Previous experimental studies about twisted MoS$_2$ have mainly focused on low-frequency Raman modes and the changes in optical properties of samples grown by chemical vapor deposition (CVD),[20] which proves the twist angle dependence of interlayer coupling. The optoelectronic properties of bilayer MoS$_2$ are modified by the twist angle due to the changes of interlayer coupling. Therefore, the photoelectric properties of bilayer MoS$_2$ can be effectively adjusted by changing its twist angle.

Applying strain to tune the crystal lattice and band structure is an important strategy to enhance the photoluminescence (PL) performance of 2D materials. MoS$_2$ can bear relatively large strain before rupturing.[23] The Raman and PL spectroscopy measurements have become standard characterization techniques for studying the properties of 2D materials, including the effects of strain[24,25] and doping/defects,[26,27] due to their nondestructive and highly sensitive nature to layer thickness.[28] In this work, the effects of tBLMs with different twist angles (θ = 0°, 5°, 30°, and 60°) under uniaxial tensile strain were revealed by Raman and PL spectra. It is found that the redshift rate of the PL peak in tBLM reaches its extreme value when θ is 30°. We then constructed the phototransistor based on 30° tBLM structure and found that the photoresponsivity is 13.05 mA W^{-1} and the specific photodetectivity is 1.83×10^7 Jones, both of which were significantly improved compared with the phototransistor based on 0° tBLM structure. These results contribute to a better understanding of the twist angle and strain effect optoelectronic properties of MoS$_2$, providing a reference for structural design to improving the optoelectronic performance of 2D material-based devices.

2. Experimental Section

2.1. Preparation of tBLM

Monolayer MoS_2 was prepared by the standard mechanical exfoliation of MoS_2 bulk material using the scotch tape technique. MoS_2 monolayers with smooth straight edges were used to make tBLMs. The layer number was verified by Raman spectra. The dry transfer method was used to stack two mechanically exfoliated MoS_2 to prepare tBLM samples onto a flexible PET (ethylene terephthalate) substrate. This method allows the preparation of tBLM samples of the desired twist angle within the accuracy of 1° using a micromanipulation stage. In addition, this technique significantly reduces any contamination between the two layers, thus ensuring robust and repeatable equipment performance.

Figure 1a–d shows the bilayer configurations with different twist angles: $\theta = 0°$, 5°, 30°, and 60°, respectively. The reason for choosing a 5° angle as the research object is that Yuan et al. found that so-called flat bands emerge when the twist angle is sufficiently tiny (smaller than 7.3°).[29] Although as a property of electronic states the flat band is not well characterized by optical means, it can also show that it is an interesting angle worthy of study. Considering the precision control of the twist angle and observing the schematic diagram of the atomic arrangement, as shown in Figure 1e, when the twist angle is 5°, a relatively obvious hexagonal pattern will appear. Therefore, 5° is chosen as one of the research objects. Dresselhaus et al. found that the PL intensity ratio of the trion and exciton reaches its maximum value for the twist angle 0° or 60°, whereas for the twist angle 30° the situation is the opposite.[30] It shows that these three angles are also relatively special and worth studying, so we also choose 0°, 30°, and 60° as the research objects. Figure 1f,g shows the schematic diagrams of the atomic arrangement with the twisted angles of 30° and 60°, respectively, showing obvious circular and parallelogram patterns.

Due to the D_{3h} symmetry of the single-layer MoS_2, the properties of tBLMs with twist angles of 60°−α and 60°+α are the same. In other words, the performance of tBLM exhibits a 60° change period. Therefore, the twist angle is limited between 0° and 60° in this work. The top layer Mo (S) atoms are aligned with the bottom layer S (Mo) atoms at the twist angle of 60°, which is the natural 2H configuration.[28]

2.2. Linear Displacement Setup

We have selected linear stretching because, unlike bending geometry, it allows the position of the sample under study to remain almost unchanged during strain loading/unloading. The fabrication of controllably uniaxial strained devices starts by developing a side-mounted micrometer onto a single-axis translation stage, as presented in Figure 1h, to provide tunable strain through the flexible substrate. The gap between the movable and fixed part of our homemade strain stage was set as 2000 μm. The flexible substrate with the tBLM sample was clamped onto the stage to prevent relative slippage from occurring between them. The minimum stroke of the helical micrometer is 10 μm. By manually controlling the movable part, the PET substrate can be stretched and strain on the tBLM samples can be applied. By comparing the high-resolution microscopic photographs of the tBLM sample before and after strain, it was determined that a strain accuracy of 0.5% could be obtained.
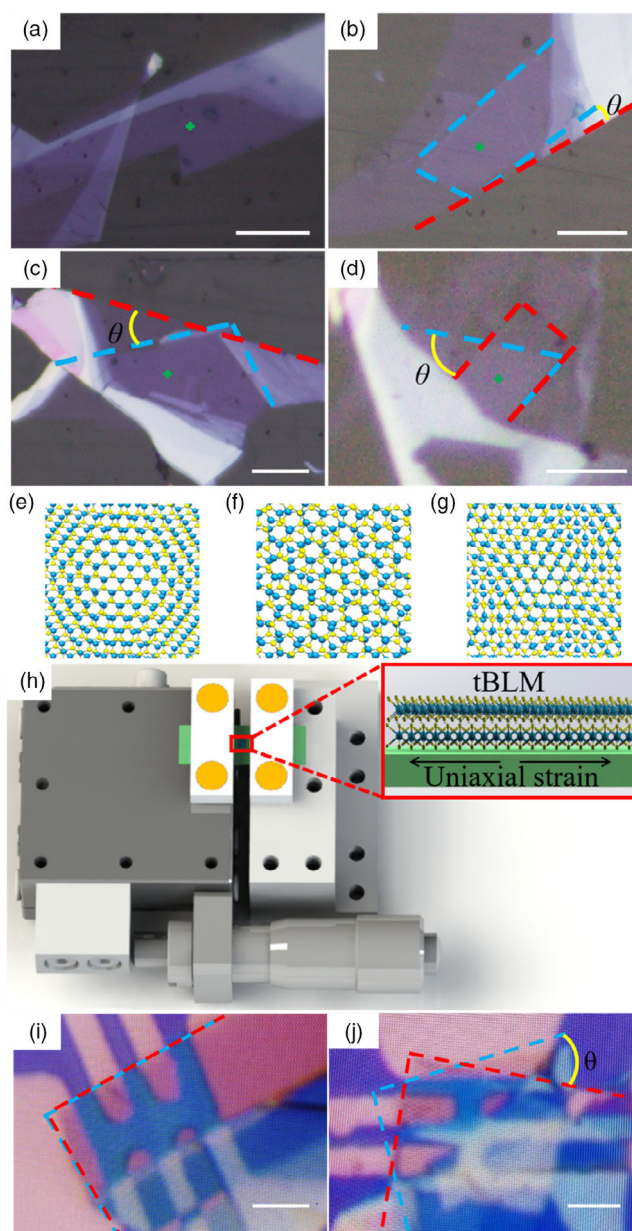

Figure 1. a–d) Optical microscope images of the MoS_2 bilayer regions with $\theta = 0°$, 5°, 30°, and 60°. The twist angle is defined as the relative rotation between two straight edges. The blue (red) lines outline the bottom (top) layer of tBLM. The green cross shows the location of the laser spot. Scale bar, 10 μm. e–g) Schematic of atom arrangement in tBLM with $\theta = 5°$, 30°, and 60°. Blue (yellow) balls correspond to Mo (S) atoms. h) Self-made linear displacement setup for uniaxial tensile strain experiments on 2D materials. i,j) Optical microscope images of the tBLM phototransistors with $\theta = 0°$ and 30°, respectively. The blue (red) lines outline the bottom (top) layer of tBLM. Scale bar, 10 μm.

2.3. Raman and PL Spectroscopy

Raman and PL spectra of tBLM flakes were done using a Witec alpha 300 R system at room temperature. The 532 nm laser with laser power of less than 1 mW was employed as the excitation source for spectroscopy measurement.

2.4. Device Fabrication

As shown in Figure 1i,j, the tBLM phototransistors were fabricated on SiO_2 (285 nm) substrate, and p^+-Si was used as the back gate electrode. The source/drain contacts were fabricated by Au/Cr metal stacks with the thickness of 50 and 5 nm.

3. Results and Discussion

Figure 2 displays the Raman spectra of tBLM samples with different twist angles under uniaxial tensile strain. With the increase in applied strain, the in-plane vibrational mode softens and manifests with the redshift of E_{2g}^1 Raman mode and splits into E_{2g}^+ and E_{2g}^- modes corresponding to in-plane atomic vibrations. However, the position of out-plane A_{1g} mode shows no measurable shift. The applied strain deforms the crystal lattice and breaks the symmetry of the crystal. The breaking of crystal symmetry causes atoms to deviate from their equilibrium positions and changes phonon modes. With the increasing strain, the E_{2g}^- peak parallel to the direction of applied strain shifts significantly toward the lower Raman wavenumber, whereas the E_{2g}^+ peak perpendicular to the direction of applied strain shifts slightly toward the opposite direction.[23,31] Compared with previous studies, the redshift rates and values of tBLM Raman peaks show a significant angle dependence.[23] As the lattice arrangement of tBLM becomes irregular and the cracks gradually appear, the linewidth in Figure 2 increases. The observed blueshift in Figure 2a may be caused by strain relaxation, which is formed at high strain levels. The tBLM films partially resist the further increase of internal strain by generating wrinkles or cracks. Although the E_{2g}^1 Raman mode of 30° tBLM is split, the separations of the E_{2g}^+ and E_{2g}^- modes are very small, unlike the tBLM of 0°, 5°, and 60°. During multiple stretching/releasing cycles, tBLMs did not slide on the substrate and did not produce obvious defects, indicating that they had good contact with the substrate.
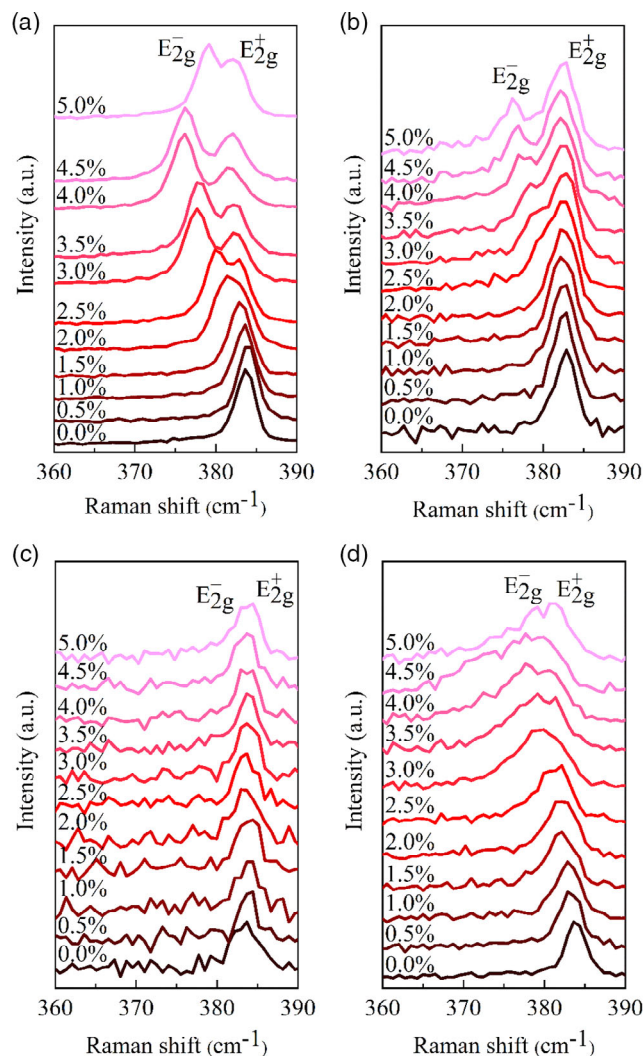

Figure 2. Raman spectra of tBLMs with increasing strain. All the spectra are shifted vertically for clarity. The twist angle of tBLMs corresponds to a) $\theta = 0°$, b) $\theta = 5°$, c) $\theta = 30°$, and d) $\theta = 60°$, respectively.
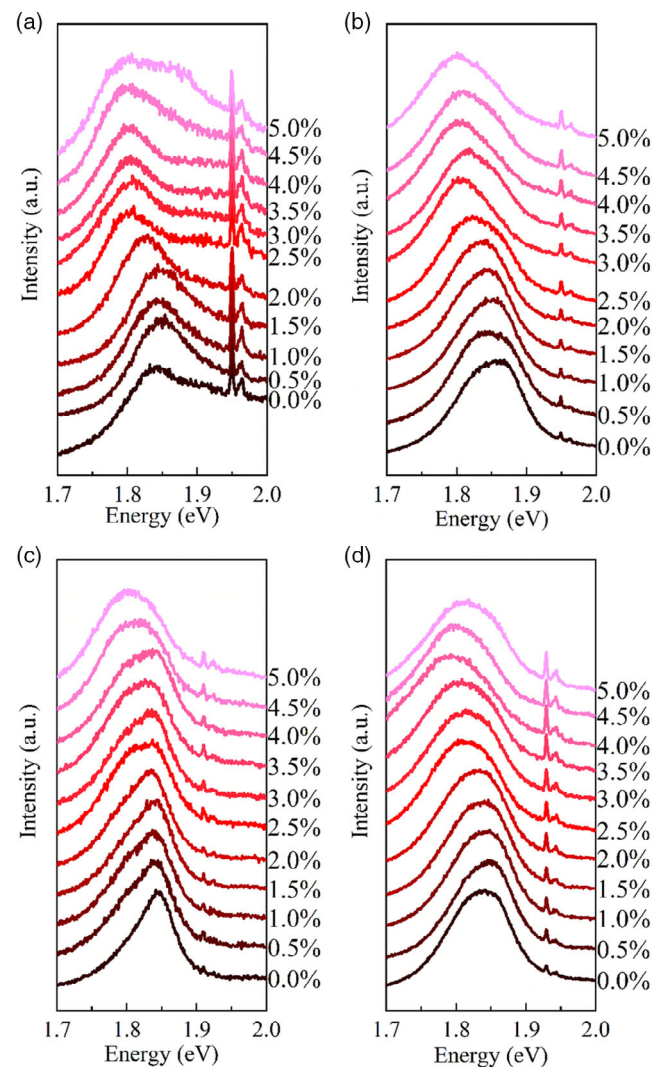

Figure 3. The PL spectra of tBLMs with increasing strain. All the spectra are shifted vertically for clarity. The twist angle of tBLMs corresponds to a) $\theta = 0°$, b) $\theta = 5°$, c) $\theta = 30°$, and d) $\theta = 60°$, respectively.

ADVANCED
SCIENCE NEWS
www.advancedsciencenews.com

physica
status
solidi
pss rrl
www.pss-rapid.com

As shown in **Figure 3**, we measured the PL spectra of four kinds of tBLMs under uniaxial tensile strain. With the strain increase, the PL peaks of all the four tBLMs show a redshift tendency. The change of exciton-binding energy of MoS_2 is negligible under strain, which has been proved both in theory and in experiment.[31] Therefore, the change of bandgap is the main reason for the observed PL peak shift. With the applied strain, the redshift per unit strain of the PL energy is at a rate of -13.24 meV/% for $\theta = 0°$, -10.62 meV/% for $\theta = 5°$,

-8.01 meV/% for $\theta = 30°$, and -10.98 meV/% for $\theta = 60°$, respectively. The redshift per unit strain of the PL energy in tBLM reaches its extreme when θ is 30°. The observed redshift of the PL peak indicates that the reduction of the bandgap in tBLMs is caused by the applied strain. As the strain increases, the position and intensity of a peak shift toward lower values. These variations of the PL properties should be attributed to the change of interlayer coupling of tBLMs as a function of twist angle and strain. For $\theta = 0°$, the separation of the adjacent layers
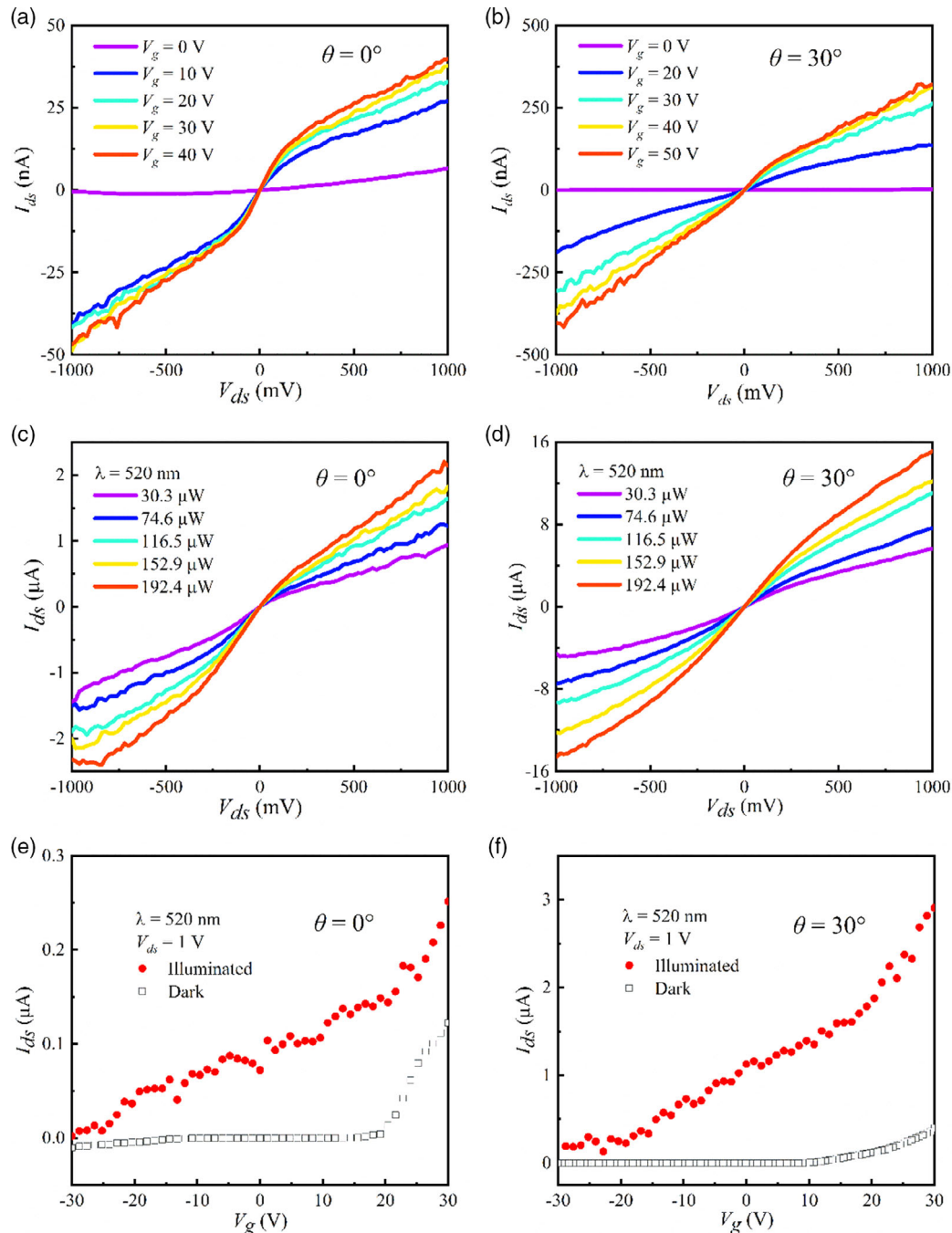

Figure 4. Comparison of photoelectric performance in tBLM phototransistors. a,b) Output characteristic curves without light. c,d) Output characteristic curves under the light of different power. e,f) Transfer characteristic curves with and without light.

ADVANCED SCIENCE NEWS
www.advancedsciencenews.com

pss rrl
physica status solidi
www.pss-rapid.com

in tBLM achieves the minimum value, because the internal S atoms are staggered. In contrast, for $\theta = 30°$, the S atoms in the top and bottom layers are arranged almost vertically, and the layer separation is in a maximum. For any other twist angle, the layer separation of tBLM is between these two extremes. In addition, the interlayer interaction also has an important effect on the electronic structure of tBLM.

It is known that band structures of bilayers evolve with the twist angles. The PL spectra taken at room temperature are dominated by a broad resonance with redshift in energy. The angle-dependent Raman and PL spectra further indicate that uniaxial strain is responsible for in-plane polarization in MoS_2. To optimize the design of MoS_2 nanostructures to improve the optoelectronic performance of tBLM-based devices, we then fabricated phototransistors for further study.

The earlier research shows that the structures of 0°-twisted-tBLM and 30°-twisted-tBLM are more representative, so the photoelectric performance of the phototransistors based on them was further investigated. The output characteristic curves of the phototransistors under different gate voltages without light are shown in **Figure 4**a,b. In the figures, the abscissa represents the source–drain voltage (V_{ds}) and the ordinate represents the source–drain current (I_{ds}). The symmetry of the current with respect to the origin at positive and negative biases indicated that a good ohmic contact was formed between the Au/Cr electrode and the tBLM channels. For the transistor with 30°-twisted-tBLM structure, the I_{ds} current is improved by ≈ 9 times than that of 0° twist one. Further, we used a xenon lamp to excite photogenerated carriers in the wavelength range of 0–1000 nm and found the best effect at 520 nm. Therefore, the 520 nm laser was used as the excitation light. Figure 4c,d shows the output characteristic curves under light with different powers, reflecting that the number of photogenerated carriers changed significantly with the change of the excitation light power. In addition, the transfer characteristic curves in the dark and under illumination were studied, as shown in Figure 4e,f. The photoresponsivity (R) and the specific photodetectivity (D^*) of the tBLM phototransistors can be calculated based on the previous data.

$$R = \frac{I_{illumination} - I_{dark}}{P} \tag{1}$$

$$D^* = \frac{R\sqrt{A}}{\sqrt{2eI_{dark}}} \tag{2}$$

Here, P is the incident laser power and A is the area of the channel.

The photoresponsivity of the 30°-twisted-tBLM-based phototransistor was 13.05 mA W^{-1}, compared with the 0.67 mA W^{-1} of the 0°-twisted-tBLM-based phototransistor. In addition, the specific photodetectivity of the tBLM phototransistor was enhanced from 1.69×10^6 to 1.83×10^7 Jones. The photoresponsivity and the specific photodetectivity of the 30°-twisted-tBLM-based phototransistor have been improved by ≈ 20 and ≈ 100 times than those values of the 0°-twisted one, respectively.

4. Conclusion

In conclusion, the optical properties of the twisted bilayer MoS_2 have been investigated under a wide range of uniaxial tensile strains using a self-made linear displacement setup. The decrease of optical bandgap in tBLM changes approximately linearly with strain. It is found that the redshift rate of the PL peak in tBLM reaches its extreme value when θ is 30°. We then constructed the phototransistor based on a 30°-twisted-tBLM structure and found that its photoresponsivity is 13.05 mA W^{-1} and its specific photodetectivity is 1.83×10^7 Jones, both of which were significantly improved compared with the 0°-twisted one. The potential applications of strain-dependent PL of tBLMs and the similar materials include tunable photonic devices and nanoscale stress sensors. The findings in this work can help to better understand the effects of twist angle and strain on the optical and electrical applications of tBLM and provide references for the design and optimization of MoS_2 nanostructures to improving the performance of optoelectronic devices based on 2D materials.

Conflict of Interest

The authors declare no conflict of interest.

Data Availability Statement

The data that support the findings of this study are available from the corresponding author upon reasonable request.

[1] S. L. Zhao, E. Q. Wang, E. A. Uzer, S. F. Guo, R. S. Qi, J. Y. Tan, K. Watanabe, T. Taniguchi, T. Nilges, P. Gao, Y. B. Zhang, H. M. Cheng, B. L. Liu, X. L. Zou, F. Wang, *Nat. Commun.* **2021**, *12*, 3947.

**ADVANCED
SCIENCE NEWS**

www.advancedsciencenews.com

pss rrl
physica status solidi

www.pss-rapid.com

[2] J. Choi, M. Florian, A. Steinhoff, D. Erben, K. Tran, D. S. Kim, L. Y. Sun, J. M. Quan, R. Claassen, S. Majumder, J. A. Hollingsworth, T. Taniguchi, K. Watanabe, K. Ueno, A. Singh, G. Moody, F. Jahnke, X. Q. Li, *Phys. Rev. Lett.* **2021**, *126*, 047401.

[3] J. E. Zimmermann, M. Axt, F. Mooshammer, P. Nagler, C. Schuller, T. Korn, U. Hofer, G. Mette, *ACS Nano* **2021**, *15*, 14725.

[4] M. Yankowitz, S. Chen, H. Polshyn, Y. Zhang, K. Watanabe, T. Taniguchi, D. Graf, A. F. Young, C. R. Dean, *Science* **2019**, *363*, 1059.

[5] W. Yao, E. Wang, C. Bao, Y. Zhang, K. Zhang, K. Bao, C. K. Chan, C. Chen, J. Avila, M. C. Asensio, J. Zhu, S. Zhou, *Proc. Natl. Acad. Sci. USA* **2018**, *115*, 6928.

[6] R. Debnath, I. Maity, R. Biswas, V. Raghunathan, M. Jain, A. Ghosh, *Nanoscale* **2020**, *12*, 17272.

[7] K. Kim, A. DaSilva, S. Huang, B. Fallahazad, S. Larentis, T. Taniguchi, K. Watanabe, B. J. LeRoy, A. H. MacDonald, E. Tutuc, *Proc. Natl. Acad. Sci. USA* **2017**, *114*, 3364.

[8] Y. Cao, V. Fatemi, S. Fang, K. Watanabe, T. Taniguchi, E. Kaxiras, P. Jarillo-Herrero, *Nature London* **2018**, *556*, 43.

[9] G. Chen, L. L. Jiang, S. Wu, B. Lyu, H. Y. Li, B. L. Chittari, K. Watanabe, T. Taniguchi, Z. W. Shi, J. Jung, Y. B. Zhang, F. Wang, *Nat. Phys.* **2019**, *15*, 237.

[10] H. Yoo, R. Engelke, S. Carr, S. A. Fang, K. Zhang, P. Cazeaux, S. H. Sung, R. Hovden, A. W. Tsen, T. Taniguchi, K. Watanabe, G. Yi, M. Kim, M. Luskin, E. B. Tadmor, E. Kaxiras, P. Kim, *Nat. Mater.* **2019**, *18*, 448.

[11] A. Kerelsky, L. J. McGilly, D. M. Kennes, L. Xian, M. Yankowitz, S. W. Chen, K. Watanabe, T. Taniguchi, J. Hone, C. Dean, A. Rubio, A. N. Pasupathy, *Nature London* **2019**, *572*, 95.

[12] Y. Xie, B. Lian, B. Jack, X. Liu, C. L. Chiu, K. Watanabe, T. Taniguchi, B. A. Bernevig, A. Yazdani, *Nature London* **2019**, *572*, 101.

[13] Y. Jiang, X. Lai, K. Watanabe, T. Taniguchi, K. Haule, J. Mao, E. Y. Andrei, *Nature London* **2019**, *573*, 91.

[14] S. Deng, Y. Zhang, L. J. Li, *Appl. Surf. Sci.* **2019**, *476*, 308.

[15] Y. L. Yu, G. S. Jung, C. Z. Liu, Y. C. Lin, C. M. Rouleau, M. Yoon, G. Eres, G. Duscher, K. Xiao, S. Irle, A. A. Puretzky, D. B. Geohegan, *ACS Nano* **2021**, *15*, 4504.

[16] V. Vitale, K. Atalar, A. A. Mostofi, J. Lischner, *2D Mater.* **2021**, *8*, 045010.

[17] T. Mueller, E. Malic, *npj 2D Mater. Appl.* **2018**, *2*, 29.

[18] W. Choi, N. Choudhary, G. H. Han, J. Park, D. Akinwande, Y. H. Lee, *Mater. Today* **2017**, *20*, 116.

[19] S. Manzeli, D. Ovchinnikov, D. Pasquier, O. V. Yazyev, A. Kis, *Nat. Rev. Mater.* **2017**, *2*, 17033.

[20] X. Zhang, R. Zhang, Y. Zhang, T. Jiang, C. Deng, X. Zhang, S. Qin, *Opt. Mater.* **2019**, *94*, 213.

[21] M. H. Naik, M. Jain, *Phys. Rev. Lett.* **2018**, *121*, 266401.

[22] S. Zhu, H. T. Johnson, *Nanoscale* **2018**, *10*, 20689.

[23] W. B. Zhang, F. H. Cheng, J. W. Huang, H. T. Yuan, Q. Wang, *Phys. Lett. A* **2021**, *418*, 127709.

[24] C. Ernandes, L. Khalil, H. Henck, M. Q. Zhao, J. Chaste, F. Oehler, A. T. C. Johnson, M. C. Asensio, D. Pierucci, M. Pala, J. Avila, A. Ouerghi, *Nanomaterials* **2021**, *11*, 2921.

[25] C. D. Mendoza, I. J. Califrer, F. L. Freire, *Appl. Surf. Sci.* **2021**, *544*, 148884.

[26] X. Chen, M. L. Lin, X. Cong, Y. C. Leng, X. Zhang, P. H. Tan, *Carbon* **2021**, *185*, 282.

[27] M. Sharma, S. Rani, D. K. Pathak, R. Bhatia, R. Kumar, I. Sameera, *Carbon* **2021**, *184*, 437.

[28] K. F. Mak, C. Lee, J. Hone, J. Shan, T. F. Heinz, *Phys. Rev. Lett.* **2010**, *105*, 136805.

[29] Y. P. Zhang, Z. Zhan, F. Guinea, J. A. Silva-Guillen, S. J. Yuan, *Phys. Rev. B* **2020**, *102*, 235418.

[30] S. X. Huang, X. Ling, L. B. Liang, J. Kong, H. Terrones, V. Meunier, M. S. Dresselhaus, *Nano Lett.* **2014**, *14*, 5500.

[31] N. Y. Tang, C. Du, Q. Q. Wang, H. R. Xu, *Microelectron. Eng.* **2020**, *223*, 111202.